Measurements of Double-Polarized Compton Scattering Asymmetries and Extraction of the Proton Spin Polarizabilities

P. P. Martel *et al.* (A2 Collaboration at MAMI)

Measurements of Double-Polarized Compton Scattering Asymmetries and Extraction of the Proton Spin Polarizabilities

P. P. Martel,[1,2,3,*] R. Miskimen,[1,†] P. Aguar-Bartolome,[2] J. Ahrens,[2] C. S. Akondi,[4] J. R. M. Annand,[5] H. J. Arends,[2] W. Barnes,[1] R. Beck,[6] A. Bernstein,[7] N. Borisov,[8] A. Braghieri,[9] W. J. Briscoe,[10] S. Cherepnya,[11] C. Collicott,[12,13] S. Costanza,[9] A. Denig,[2] M. Dieterle,[14] E. J. Downie,[2,5,10] L. V. Fil'kov,[11] S. Garni,[14] D. I. Glazier,[5,15] W. Gradl,[2] G. Gurevich,[16] P. Hall Barrientos,[15] D. Hamilton,[5] D. Hornidge,[3] D. Howdle,[5] G. M. Huber,[17] T. C. Jude,[15] A. Kaeser,[14] V. L. Kashevarov,[11] I. Keshelashvili,[14] R. Kondratiev,[16] M. Korolija,[18] B. Krusche,[14] A. Lazarev,[8] V. Lisin,[16] K. Livingston,[5] I. J. D. MacGregor,[5] J. Mancell,[5] D. M. Manley,[4] W. Meyer,[19] D. G. Middleton,[2,3] A. Mushkarenkov,[1] B. M. K. Nefkens,[20,‡] A. Neganov,[8] A. Nikolaev,[6] M. Oberle,[14] H. Ortega Spina,[2] M. Ostrick,[2] P. Ott,[2] P. B. Otte,[2] B. Oussena,[2] P. Pedroni,[9] A. Polonski,[16] V. Polyansky,[11] S. Prakhov,[2,10,20] A. Rajabi,[1] G. Reicherz,[19] T. Rostomyan,[14] A. Sarty,[13] S. Schrauf,[2] S. Schumann,[2] M. H. Sikora,[15] A. Starostin,[20] O. Steffen,[2] I. I. Strakovsky,[10] T. Strub,[14] I. Supek,[18] M. Thiel,[21] L. Tiator,[2] A. Thomas,[2] M. Unverzagt,[2,6] Y. Usov,[8] D. P. Watts,[15] L. Witthauer,[14] D. Werthmüller,[14] and M. Wolfes[2]

(A2 Collaboration at MAMI)

[1]*Department of Physics, University of Massachusetts Amherst, Amherst, Massachusetts 01003, USA*
[2]*Institut für Kernphysik, Universität Mainz, D-55099 Mainz, Germany*
[3]*Department of Physics, Mount Allison University, Sackville, New Brunswick E4L 1E6, Canada*
[4]*Department of Physics, Kent State University, Kent, Ohio 44242, USA*
[5]*SUPA School of Physics and Astronomy, University of Glasgow, Glasgow G12 8QQ, UK*
[6]*Helmholtz-Institut für Strahlen- und Kernphysik, Universität Bonn, D-53115 Bonn, Germany*
[7]*Laboratory for Nuclear Science, Massachusetts Institute of Technology, Cambridge, Massachusetts 02139, USA*
[8]*Joint Institute for Nuclear Research (JINR), 141980 Dubna, Russia*
[9]*INFN Sezione di Pavia, I-27100 Pavia, Italy*
[10]*Department of Physics, The George Washington University, Washington, DC 20052, USA*
[11]*Lebedev Physical Institute, 119991 Moscow, Russia*
[12]*Department of Physics and Atmospheric Science,*
Dalhousie University, Halifax, Nova Scotia B3H 4R2, Canada
[13]*Department of Astronomy and Physics, Saint Marys University, Halifax, Nova Scotia B3H 3C3, Canada*
[14]*Departement Physik, Universität Basel, CH-4056 Basel, Switzerland*
[15]*School of Physics, University of Edinburgh, Edinburgh EH9 3JZ, UK*
[16]*Institute for Nuclear Research, 125047 Moscow, Russia*
[17]*Department of Physics, University of Regina, Regina, Saskatchewan S4S 0A2, Canada*
[18]*Rudjer Boskovic Institute, HR-10000 Zagreb, Croatia*
[19]*Institut für Experimentalphysik, Ruhr-Universität, D-44780 Bochum, Germany*
[20]*Department of Physics and Astronomy, University of California Los Angeles, Los Angeles, California 90095-1547, USA*
[21]*II. Physikalisches Institut, Universität Giessen, D-35392 Giessen, Germany*
(Dated: February 17, 2015)

The spin polarizabilities of the nucleon describe how the spin of the nucleon responds to an incident polarized photon. The most model-independent way to extract the nucleon spin polarizabilities is through polarized Compton scattering. Double-polarized Compton scattering asymmetries on the proton were measured in the $\Delta(1232)$ region using circularly polarized incident photons and a transversely polarized proton target at the Mainz Microtron. Fits to asymmetry data were performed using a dispersion model calculation and a baryon chiral perturbation theory calculation, and a separation of all four proton spin polarizabilities in the multipole basis was achieved. The analysis based on a dispersion model calculation yields $\gamma_{E1E1} = -3.5 \pm 1.2$, $\gamma_{M1M1} = 3.16 \pm 0.85$, $\gamma_{E1M2} = -0.7 \pm 1.2$, and $\gamma_{M1E2} = 1.99 \pm 0.29$, in units of 10^{-4} fm^4.

Electromagnetic polarizabilities are fundamental properties of composite systems such as molecules, atoms, nuclei, and hadrons [1]. Whereas magnetic moments provide information about the ground-state properties of a system, polarizabilities provide information about the excited states of the system. For atomic systems, polarizabilities are of the order of the atomic volume. For hadrons, polarizabilities are much smaller than the volume, typically of order 10^{-4} fm^3, because of the greater strength of the QCD force as compared to the electromagnetic force. Extracted polarizabilities can provide a

* martel@kph.uni-mainz.de
† miskimen@physics.umass.edu
‡ deceased

guide by favoring, or disfavoring, models of hadron structure and QCD.

Hadron polarizabilities are best extracted with Compton scattering experiments, where the polarizabilities cause a deviation of the cross section from the prediction of Compton scattering off a structureless Dirac particle. In the energy expansion of the nuclear Compton scattering amplitude, the $\mathcal{O}(\omega^2)$ term depends on the electric and magnetic, or scalar, polarizabilities of the nucleon, α and β, respectively, and the $\mathcal{O}(\omega^3)$ term depends on the spin polarizabilities of the nucleon, where ω is the incident photon energy. The $\mathcal{O}(\omega^3)$ term in the amplitude is [2] an effective spin-dependent interaction,

$$H_{\text{eff}}^{(3)} = -4\pi\left[\frac{1}{2}\gamma_{E1E1}\vec{\sigma}\cdot(\vec{E}\times\dot{\vec{E}}) + \frac{1}{2}\gamma_{M1M1}\vec{\sigma}\cdot(\vec{H}\times\dot{\vec{H}}) \right.$$
$$\left. - \gamma_{M1E2}E_{ij}\sigma_i H_j + \gamma_{E1M2}H_{ij}\sigma_i E_j\right], \quad (1)$$

which describes the coupling of the proton spin, $\vec{\sigma}$, with an applied electric, $\vec{E}$, or magnetic, $\vec{H}$, field and their time derivatives, $\dot{\vec{E}} = \partial_t\vec{E}$, and space derivatives, $E_{ij} = \frac{1}{2}(\nabla_i E_j + \nabla_j E_i)$, in the multipole basis, where $\gamma_{X\lambda Y\lambda'}$ is the spin polarizability for incident and final photon multipolarities $X\lambda$ and $Y\lambda'$. Because the spin polarizability effect varies as ω^3, the sensitivity to the spin polarizabilities, relative to that of α and β, is greatest in Compton scattering reactions in the $\Delta(1232)$ region, but below the threshold for double-pion photoproduction where additional terms complicate matters.

Several experiments have provided constraints on linear combinations of the proton spin polarizabilities. The most important of these are (i) the forward spin polarizability γ_0, which comes from a set of two experiments of the GDH Collaboration, [3, 4], $\gamma_0 = -\gamma_{E1E1} - \gamma_{E1M2} - \gamma_{M1E2} - \gamma_{M1M1} = (-1.01 \pm 0.08 \pm 0.10) \times 10^{-4}\ \text{fm}^4$, and (ii) the backward spin polarizability γ_π, which was determined from an analysis of backward angle Compton scattering [5], $\gamma_\pi = -\gamma_{E1E1} - \gamma_{E1M2} + \gamma_{M1E2} + \gamma_{M1M1} = (8.0 \pm 1.8) \times 10^{-4}\ \text{fm}^4$. The convention followed here is to subtract the structureless pion-pole contribution from the spin polarizability; the pole term is present in γ_π and the multipole basis spin polarizabilities, [2] but is not present in γ_0. Table I presents the results from several theoretical calculations for the spin polarizabilities, showing the wide range of theoretical predictions.

Compton scattering asymmetries in the $\Delta(1232)$ region have sensitivity to the spin polarizabilities [15], with the relationship described in Eqs. (3.23), (3.26), and (3.15) of Ref. [2]. This Letter presents the first measurements of double-polarized Compton scattering asymmetries on the nucleon at energies below the double-pion photoproduction threshold, and the first analysis of Compton scattering asymmetries for the determination of all four spin polarizabilities. The double-polarization asymmetry with circularly polarized incident photons on a transversely polarized proton target, Σ_{2x}, was measured using the Crystal Ball detector [16] at the Mainz

Microtron (MAMI) [17]. A GaAsP (III-V semiconductor) source was used to produce a longitudinally polarized electron beam, with the polarization measured via a Mott polarimeter [18]. The average beam polarization was $81.9 \pm 0.1\%$. To remove systematic effects, the helicity of the beam was automatically flipped at a frequency of about 1 Hz. The 450 MeV electron beam produced by the MAMI accelerator was passed through a 10 μm Cu radiator, producing a circularly polarized Bremsstrahlung photon beam. The energy of the radiated photon was determined via the detection of the scattered electron in the Glasgow photon tagger [19], and only photons in the range of $E_\gamma = 273 - 303$ MeV were used in this analysis. After collimation by a 2.5 mm diameter lead collimator, the photon beam impinged on a frozen spin butanol target [20]. The target was polarized by dynamic nuclear polarization [21], typically up to initial values of 90% with relaxation times on the order of 1000 hours. Proton polarizations were measured using an NMR coil at the beginning and end of a polarization period, with an average of $81.6 \pm 1.7\%$. To further remove systematic effects, the direction of proton polarization was reversed several times, typically once per week of experiment running time.

To remove backgrounds from interactions of the photon beam with the material of the cryostat and non-hydrogen nucleons in the target and He bath, separate data were taken using a carbon foam target with density 0.55 g/cm^3. The density of the carbon foam was such that a cylinder of identical geometric size to the butanol target provided a close approximation to the number of non-hydrogen nucleons in the butanol target, allowing for a simple 1:1 subtraction accounting only for differences in luminosity.

Final-state particles were detected in the Crystal Ball (CB) [16] and TAPS [22] detectors, both of which are outfitted with charged particle identification systems [23]. Together these detectors cover 97% of 4π sr. Events were selected where a single neutral and a single charged cluster of detector element hits, both with energies above 15 MeV, were observed in coincidence with an event in the photon tagger. A prompt timing selection was applied followed by an accidental coincidence subtraction. An additional level of background suppression was achieved by requiring a projected angle of less than 10° between the measured direction of the charged particle and the direction of the proton recoil predicted by the Compton scattering kinematics. The 10° opening angle requirement was determined through simulation and checked with π^0 photoproduction data.

The ratio of π^0 photoproduction to Compton scattering cross sections in the $\Delta(1232)$ region is approximately 100:1. Even with the exclusivity selection, accidental subtraction, and opening angle requirement, π^0 backgrounds remained in the data, as shown in the missing-mass spectrum of Fig. 1. Typically, these backgrounds were from π^0 events in which a low-energy decay photon escaped detection by passing up or down the beam-

	$O(\epsilon^3)$	$O(p^4)_a$	$O(p^4)_b$	K-matrix	HDPV	DPV	L_χ	HBχPT	BχPT	Experiment
γ_{E1E1}	−1.9	−5.4	1.3	−4.8	−4.3	−3.8	−3.7	−1.1 ± 1.8 (th)	−3.3	−3.5 ± 1.2
γ_{M1M1}	0.4	1.4	3.3	3.5	2.9	2.9	2.5	2.2 ± 0.5 (st) ± 0.7 (th)	3.0	3.16 ± 0.85
γ_{E1M2}	0.7	1.0	0.2	−1.8	−0.02	0.5	1.2	−0.4 ± 0.4 (th)	0.2	−0.7 ± 1.2
γ_{M1E2}	1.9	1.0	1.8	1.1	2.2	1.6	1.2	1.9 ± 0.4 (th)	1.1	1.99 ± 0.29
γ_0	−1.1	1.9	−3.9	2.0	−0.8	−1.1	−1.2	−2.6	−1.0	−1.01 ± 0.08 ± 0.10 [3, 4]
γ_π	3.5	6.8	6.1	11.2	9.4	7.8	6.1	5.6	7.2	8.0 ± 1.8 [5]

TABLE I. Spin polarizabilities in units of $10^{-4}\,\mathrm{fm}^4$. $O(\epsilon^3)$ is a small scale expansion calculation [6]. $O(p^4)_{a,b}$ are chiral perturbation theory calculations [7, 8]. The K-matrix calculation is from Ref. [9]. HDPV and DPV are fixed-t [10, 15] and fixed-angle [11] dispersion relation calculations, respectively. L_χ is a chiral lagrangian calculation [12]. HBχPT and BχPT are heavy baryon and covariant, respectively, chiral perturbation theory calculations with $\Delta(1232)$ degrees of freedom [13, 14]. Experimental results for γ_{E1E1}, γ_{E1M2}, γ_{M1E2}, and γ_{M1M1} are from this work, using a combined analysis of Σ_{2x} and Σ_3 asymmetries using a dispersion model calculation [11].

line, or through the gap between the CB and TAPS. To isolate this background, selections were used to make the regions of reduced acceptance well defined. These regions were (i) the forward hole in the TAPS detector, $0 - 6°$, (ii) the region between TAPS and the CB, $18 - 25°$, and (iii) the backward hole in the CB, $150 - 180°$. This aggregate solid angle is referenced as Ω_{cut}. To estimate the π^0 background that resulted from decay photons entering Ω_{cut}, π^0 events were identified where both decay photons were detected, and where one of the decay photons fell into a solid angle bin adjacent to Ω_{cut}. For $\Omega_{\mathrm{cut}} = 0 - 6°$, the adjacent solid angle bin is $\Omega_{\mathrm{adj}} = 6 - 8.5°$; for $\Omega_{\mathrm{cut}} = 18 - 25°$, $\Omega_{\mathrm{adj}} = 13.2 - 27.9°$; and for $\Omega_{\mathrm{cut}} = 150 - 180°$, $\Omega_{\mathrm{adj}} = 143 - 150°$. Missing-mass spectra were calculated using

$$M_{\mathrm{miss}} = \sqrt{(E_\gamma + m_p - E_c)^2 - (\vec{p}_\gamma - \vec{p}_c)^2}, \qquad (2)$$

where E_c and $\vec{p}_c$ are the energy and momentum of the Compton photon. For the π^0 background events the photon detected in Ω_{adj} was ignored, and the second photon was treated as the Compton photon.

After removing the various background contributions shown in Fig. 1 the final missing-mass distribution is shown in Fig. 2. The subtraction of backgrounds is done separately for each helicity state, as the π^0 backgrounds themselves result in non-zero asymmetries. Monte Carlo simulation of the Compton scattering lineshape shows good agreement between data and calculation for the Compton peak, except around 980 MeV. The counts there are from an unsubtracted background due to the gap between the CB and TAPS which simulation shows would appear on the high M_{miss} side of the peak. While relatively weak at $\theta_c = 100 - 120°$, this background becomes stronger at more backward angles. The effect of the background on the asymmetry was studied by integrating the spectrum in Fig. 2 to various upper limits. Integrating to final values up to 940 MeV resulted in asymmetries consistent within uncertainties, while integrating to increasingly higher values resulted in asymmetries that varied outside of uncertainties from lower limit integrations. For this reason a relatively conservative integration limit of 940 MeV was used in this analysis.
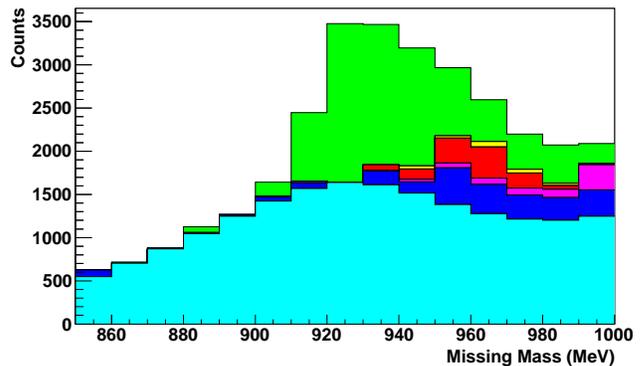

FIG. 1. Missing-mass spectra for $E_\gamma = 273 - 303$ MeV, and $\theta_c = 100 - 120°$ (color online). In addition to the actual Compton scattering distribution, each background, shown in a different color, is stacked on top of one another to show its contribution to the total initial distribution. From bottom to top; light blue is for tagger accidentals; blue is for carbon/cryostat background; magenta, red, and yellow were constructed from data to mimic where a π^0 decay photon was lost in the upstream CB hole, the region between CB and TAPS, and the downstream TAPS hole, respectively, each of which had their own accidental and carbon subtraction already applied; and green shows the final subtracted result.

Further details of this analysis can be found in Ref. [24]

For a given incoming photon energy E_γ, Compton scattering polar angle θ_c, and azimuthal angle ϕ_c relative to the target polarization direction, the asymmetry Σ_{2x} is defined by

$$\Sigma_{2x}(E_\gamma, \theta_c) = [P_T P_\gamma(E_\gamma)\cos(\phi_c)]^{-1}$$
$$\left[\frac{N^R(E_\gamma, \theta_c, \phi_c) - N^L(E_\gamma, \theta_c, \phi_c)}{N^R(E_\gamma, \theta_c, \phi_c) + N^L(E_\gamma, \theta_c, \phi_c)} \right], \quad (3)$$

where P_T is the target polarization, P_γ is the beam polarization, and N^R (N^L) are the counts in the specified bin with a right (left) helicity beam.

The measured asymmetries are plotted in Fig. 3. In addition to statistical uncertainties, the systematic uncertainties from both beam and target polarizations are incorporated in the error bars shown, though at worst are
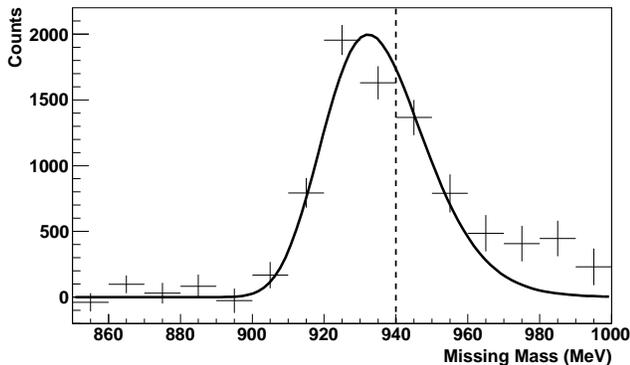
FIG. 2. Missing-mass spectrum after removing the background contributions shown in Fig. 1 for $E_\gamma = 273-303$ MeV, and $\theta_c = 100 - 120°$. The solid line is the Compton scattering lineshape determined from simulation. The dashed line indicates the upper integration limit used in the analysis.

FIG. 3. Σ_{2x} for $E_\gamma = 273 - 303$ MeV (color online). The curves are from a dispersion theory calculation [11] with α, β, γ_0, and γ_π held fixed at their experimental values, and γ_{M1M1} fixed at 2.9. From bottom to top, the green, blue, brown, red and magenta bands are for γ_{E1E1} equal to -6.3, -5.3, -4.3, -3.3, and -2.3, respectively. The width of each band represents the propagated errors from α, β, γ_0, and γ_π combined in quadrature.

Data fit	Model	γ_{E1E1}	γ_{M1M1}
Σ_{2x}	Disp	-4.6 ± 1.6	-7 ± 11
Σ_3	Disp	-1.4 ± 1.7	3.20 ± 0.85
Σ_{2x} and Σ_3	Disp	-3.5 ± 1.2	3.16 ± 0.85
Σ_{2x} and Σ_3	BχPT	-2.6 ± 0.8	2.7 ± 0.5

TABLE II. Results from fitting Σ_{2x} (this work) and Σ_3 [25] data using either a dispersion model calculation (Disp) [11] or a BχPT calculation [26].

only 9% of the total uncertainty. Systematic uncertainty from the carbon background subtraction was estimated by varying the carbon background ratio by $\pm 20\%$ from the expected value. The effect on the asymmetries was negligible, at worst about 10% of the total uncertainty, and this systematic uncertainty is not included in the error bars shown in Fig. 3. The curves are from a dispersion theory calculation [11] for values of γ_{E1E1} ranging from -6.3 to -2.3, but with γ_{M1M1} fixed at the HDPV value from Table I of 2.9 [10, 15]. The width of each band represents the propagated errors using $\alpha = 12.16 \pm 0.58$ and $\beta = 1.66 \pm 0.69$, as well as γ_0 and γ_π from Table I, combined in quadrature. The curves graphically demonstrate the sensitivity of the asymmetries to γ_{E1E1}, showing a preferred solution of $\gamma_{E1E1} \approx -4.3 \pm 1.5$. A similar analysis holding $\gamma_{E1E1} = -4.3$ fixed and allowing γ_{M1M1} to vary, shows that the asymmetries are insensitive to γ_{M1M1}.

The double-asymmetry data from this measurement and published results [25] for the single-polarization asymmetry with linearly polarized photons, Σ_3, were fitted with a dispersion model calculation [11] and a baryon chiral perturbation theory (BχPT) calculation [26]. Only asymmetry points obtained by the LEGS collaboration below double-pion photoproduction threshold were used in this analysis. The BχPT calculation includes pion, nucleon, and $\Delta(1232)$ degrees of freedom at order NNLO [26]. α, β, γ_{E1E1}, γ_{M1M1}, γ_0, and γ_π were fitted to the asymmetry data sets, and to the known constraints on $\alpha + \beta$, $\alpha - \beta$, γ_0, and γ_π. The constraint on $\alpha + \beta$ is given by the Baldin sum rule, $\alpha + \beta = 13.8 \pm 0.4$ [27], and the constraint of $\alpha - \beta = 7.6 \pm 0.9$ is taken from the analysis of Grießhammer et al. [28]

Table II shows results from data fitting. The first column gives the data set used for fitting, the second column gives the model used, and the third and fourth columns show the results for γ_{E1E1} and γ_{M1M1}. The first row shows results from fitting only the Σ_{2x} data from this
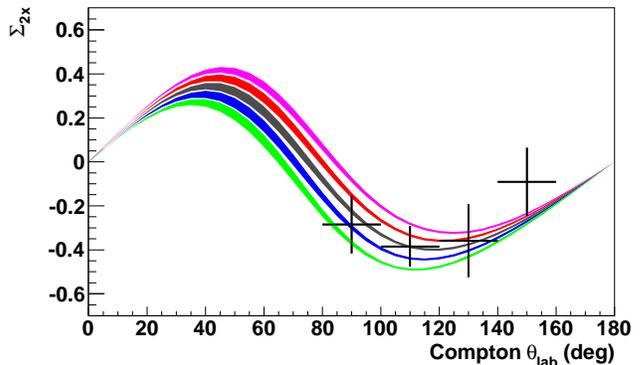
work. The result for γ_{E1E1} is in good agreement with the expectation from the graphical analysis shown in Fig. 3, and the Σ_{2x} data alone have little sensitivity to γ_{M1M1}. The second row shows results from fitting only Σ_3 [25]. Within uncertainties, the results for γ_{E1E1} from fitting Σ_{2x} and Σ_3 data separately are in approximate agreement. The third row shows the results from the combined fit of Σ_{2x} and Σ_3 using the dispersion model [11], and the fourth row shows the combined fit of Σ_{2x} and Σ_3 using the BχPT calculation [26]. Within uncertainties, the results for γ_{E1E1} and γ_{M1M1} from the two models are also in agreement. This indicates that the model dependence of the polarizability fitting is comparable to, or smaller than, the statistical errors from data fitting.

Results for all four spin polarizabilities obtained from the combined fit of Σ_{2x} and Σ_3 using the dispersion model calculation are presented in the last column in Table I, along with previous results for γ_0 and γ_π. γ_{E1M2} and γ_{M1E2} were extracted using the linear relationships of γ_0 and γ_π. The table shows generally good agreement between the extracted spin polarizabilities and the predictions of the dispersion theory calculations [10, 11, 15], the K-matrix theory calculation [9], the chiral Lagrangian calculation [12], and the chiral perturbation theory calculations [13, 14]. The size of the experimental uncertainties is too large to discriminate between these various

models.

In summary, data are presented for the double-polarized Compton scattering asymmetry with a transversely polarized proton target in the $\Delta(1232)$ region. The data have good sensitivity to the γ_{E1E1} spin polarizability. The spin polarizabilities obtained using the dispersion theory analysis [11] of the asymmetry data, and those obtained using the BχPT analysis [26] of the data, agree within uncertainties. The spin polarizabilities are in good agreement with the dispersion theory, K-matrix theory, the chiral Lagrangian calculation, and the chiral perturbation theory calculations.

[1] B. R. Holstein, Nucl. Phys. **546**, 213 (1992).
[2] D. Babusci, G. Giordano, A. I. L'vov, G. Matone, and A. M. Nathan, Phys. Rev. C **58**, 1013 (1998).
[3] J. Ahrens *et al.* (GDH and A2 Collaborations), Phys. Rev. Lett. **87**, 022003 (2001).
[4] H. Dutz, K. Helbing, J. Krimmer, T. Speckner, and G. Zeitler (GDH and A2 Collaborations), Phys. Rev. Lett. **91**, 192001 (2003).
[5] M. Camen *et al.*, Phys. Rev. C **65**, 0302202 (2002).
[6] T. R. Hemmert, B. R. Holstein, J. Kambor, and G. Knöchlein, Phys. Rev. D **57**, 5746 (1998).
[7] K. B. Vijaya Kumar, J. A. McGovern, and M. C. Birse, Phys. Lett. B **479**, 167 (2000).
[8] G. C. Gellas, T. R. Hemmert, and Ulf-G. Meißner, Phys. Rev. Lett. **85**, 14 (2000).
[9] S. Kondratyuk and O. Scholten, Phys. Rev. C **64**, 024005 (2001).
[10] B. R. Holstein, D. Drechsel, B. Pasquini, and M. Vanderhaeghen, Phys. Rev. C **61**, 034316 (2000).
[11] D. Drechsel, B. Pasquini, and M. Vanderhaeghen, Phys. Rep. **378**, 99 (2003).
[12] A. M. Gasparyan, M. F. M. Lutz, and B. Pasquini, Nucl. Phys. A **866**, 79 (2011).
[13] J. A. McGovern, D. R. Phillips, and H. W. Grießhammer, Eur. Phys. J. A **49**, 12 (2013).
[14] V. Lensky and J. McGovern, Phys. Rev. C **89**, 032202 (2014).
[15] B. Pasquini, D. Drechsel, and M. Vanderhaeghen, Phys. Rev. C **76**, 015203 (2007).
[16] A. Starostin, B. M. K. Nefkens, *et al.* (The Crystal Ball Collaboration), Phys. Rev. C **64**, 055205 (2001).
[17] K.-H. Kaiser *et al.*, Nucl. Instrum. Methods A **593**, 159 (2008).
[18] V. Tioukine, K. Aulenbacher, and E. Riehn, Rev. Sci. Instrum. **82**, 033303 (2011).
[19] J. McGeorge, J. Kellie, *et al.*, Eur. Phys. J. A **37**, 129 (2008).
[20] A. Thomas, Eur. Phys. J. Special Topics **198**, 171 (2011).
[21] D. G. Crabb and W. Meyer, Annu. Rev. Nucl. Part. Sci. **47**, 67 (1997).
[22] R. Novotny, IEEE Trans. Nucl. Sci. **38**, 379 (1991).
[23] C. M. Tarbert *et al.* (Crystal Ball at MAMI and A2 Collaborations), Phys. Rev. Lett. **100**, 132301 (2008).
[24] P. P. Martel, *Measuring Proton Spin Polarizabilities with Polarized Compton Scattering*, Ph.D. thesis, University of Massachusetts Amherst, USA (2013).
[25] G. Blanpied *et al.* (The LEGS Collaboration), Phys. Rev. C **64**, 025203 (2001).
[26] V. Lensky and V. Pascalutsa, Eur. Phys. J. C **65**, 195 (2010).
[27] V. O. de León *et al.*, Eur. Phys. J. A **10**, 207 (2001).
[28] H. W. Grießhammer, J. A. McGovern, D. R. Phillips, and G. Feldman, Prog. Part. Nucl. Phys. **67**, 841 (2012).